Visual stimulus presentation using fiber optics in the MRI scanner

Ruey-Song Huang [a,b,*], Martin I. Sereno [a]

[a] *Department of Cognitive Science, University of California San Diego, La Jolla, CA 92093-0515, USA*
[b] *Swartz Center for Computational Neuroscience, Institute for Neural Computation, University of California San Diego, La Jolla, CA 92093-0961, USA*

Abstract

Imaging the neural basis of visuomotor actions using fMRI is a topic of increasing interest in the field of cognitive neuroscience. One challenge is to present realistic three-dimensional (3-D) stimuli in the subject's peripersonal space inside the MRI scanner. The stimulus generating apparatus must be compatible with strong magnetic fields and must not interfere with image acquisition. Virtual 3-D stimuli can be generated with a stereo image pair projected onto screens or via binocular goggles. Here, we describe designs and implementations for automatically presenting physical 3-D stimuli (point-light targets) in peripersonal and near-face space using fiber optics in the MRI scanner. The feasibility of fiber-optic based displays was demonstrated in two experiments. The first presented a point-light array along a slanted surface near the body, and the second presented multiple point-light targets around the face. Stimuli were presented using phase-encoded paradigms in both experiments. The results suggest that fiber-optic based displays can be a complementary approach for visual stimulus presentation in the MRI scanner.
© 2007 Elsevier B.V. All rights reserved.

Keywords: fMRI; Fiber optics; 3-D stimuli; Peripersonal space; Near-face space

1. Introduction

Functional magnetic resonance imaging (fMRI) has become one of the most useful noninvasive technologies for mapping human brain functions. Stimulus presentation and response monitoring during fMRI experiments remain a challenging task (Savoy et al., 1999). Most fMRI experiments involve passive viewing of visual stimuli and simple button presses, whereas other visuomotor experiments involve saccades, pointing, and reaching to targets in peripersonal and near-face space (Culham and Valyear, 2006; Culham et al., 2006; Chapman et al., 2007; Filimon et al., 2007; Quinlan and Culham, 2007; Culham et al., 2008). Some experiments also involve visuomotor interaction with real objects at different depths in peripersonal space, which is difficult to simulate using projected images. Although visual stimuli can be projected onto a close-up screen in peripersonal or near-face space using an LCD video projector (Pitzalis et al., 2006; Sereno and Huang, 2006), this method has some limitations. First, it is impossible to obtain complete darkness with a video projector. A neutral density filter can darken the background, but subjects typically can still see their hands while reaching to an extinguished target against the 'black' background, resulting in a potential confound (Filimon et al., 2007, in preparation). Second, although stereoscopic depth can be simulated with red–green or polarized displays, these have limitations in stimulus range, and can be difficult to combine with real objects. Binocular goggles overcome some of these limitations (at considerable expense), but are not a complete substitute for real objects (e.g., accommodation cues are difficult to simulate, and virtual objects cannot be grasped or reached).

Alternatively, real objects or a handful of light emitting diodes (LEDs) can be placed at different depths inside the scanner bore. However, conductive wires driving the LEDs need to be properly shielded (as well demonstrated in Quinlan and Culham, 2007; Culham et al., 2008) if multiple LEDs are to be placed near the body surface in peripersonal space. Time-varying gradient magnetic fields and radio-frequency (RF) pulses, as well as small movements of unshielded wires themselves could induce currents (antenna effect) and result in heating and image artifacts (Dempsey et al., 2001; Dempsey and Condon, 2001; Meinhardt and Müller, 2001; Shellock, 2002; Armenean et al., 2004). The

* Corresponding author at: Swartz Center for Computational Neuroscience, Institute for Neural Computation, University of California San Diego, 9500 Gilman Drive #0961, La Jolla, CA 92093-0961, USA. Tel.: +1 858 458 1927; fax: +1 858 458 1847.

E-mail address: rshuang@sccn.ucsd.edu (R.-S. Huang).

induced currents can also interfere with electrical signals involving stimulus presentation or response monitoring.

An alternative method for visual stimulus presentation in near-face and peripersonal space is to use fiber optics in the MRI scanner (Cornelissen et al., 1997; Hoffman et al., 2003; Scott et al., 2003; Huang and Sereno, 2006; Chapman et al., 2007). Optical fibers are made from glass or plastics that are compatible with high magnetic fields and do not generate radio-frequency interference. Originally demonstrated as a 'light guiding' concept by John Tyndall in 1870, fiber optics has been used for numerous applications, including medical instruments (endoscopes/fiberscopes), lighting (e.g., buildings, traffic signals, dashboards, and decorations), and communications (Crisp, 2001; DeCusatis and DeCusatis, 2006; Goff, 2002). Other fiber optics applications for MRI and fMRI include lighting in the scanner bore, motor response monitoring (Meinhardt and Müller, 2001; Burdet et al., 2004; Zakzanis et al., 2005), eye tracking (Kimmig et al., 1999; Kanowski et al., 2007), eyeblink measurement (Miller et al., 2005), measurement and calibration of luminance (Strasburger et al., 2002), cardiac signals and respiratory monitoring (Lindberg et al., 1992; Brau et al., 2002; Greatbatch et al., 2002), temperature measurement (Sade and Katzir, 2001; Armenean et al., 2004), and skin conductance recording (Lagopoulos et al., 2005). In this study, we outline designs and methods for 3-D visual stimulus presentation in peripersonal and near-face space using fiber optics in the MRI scanner, and demonstrate their feasibility in two experiments.

2. Materials and methods

2.1. Design concept

The goal of our design is to present individual fiber-optic point lights (targets) at any depth inside the scanner bore, allowing subjects to point or reach to the targets in their peripersonal space. This concept is different from other approaches using fiberscopes or bundles of optical fibers for stimulus presentation or eye tracking (Cornelissen et al., 1997; Kimmig et al., 1999; Hoffman et al., 2003; Kanowski et al., 2007). In these approaches, subjects view two-dimensional images of a remote LCD or CRT display through fiberscopes. However, our aim is to present discrete targets in three-dimensional space. The design and construction of our fiber-optic stimulus presentation systems consist of three elements, including stimulus generating programs, digital circuits, and supporting structures for the fiber-optic lights. The stimulus generating programs written in ANSI C send out eight-bit transistor–transistor logic (TTL) pulses to a parallel port of a portable computer (Shuttle XPC, Taiwan) running the Linux operating system. The digital circuits decode the TTL pulses and control the timing and sequence of LEDs that illuminate individual strands of optical fibers entering the scanner bore. The supporting structures of fiber-optic lights are constructed according to the desired spatial layout of point-light targets for each experimental paradigm.

2.2. Experiment I—topographic mapping of distance

The sequential relations of sensory stimuli along a certain physical dimension (e.g., polar angle of the visual field, pitch of sound, and areas of body surface) are preserved in topographic maps on the cortical surface. The phase-encoded or traveling-wave method has revealed topographic maps of two-dimensional visual space (polar angle and eccentricity) in human fMRI experiments (Engel et al., 1994; Sereno et al., 1995). This method may be extended to map cortical representation of the third dimension of space (Huang and Sereno, 2006). Here, we constructed a fiber-optic display apparatus that presented a point-light array on a slanted surface inside the scanner bore. The array contained eight rows of four blue point lights (0.25 mm) evenly distributed on a double-layer, 40 in. × 16 in. black foam board (Figs. 1 and 2). The light array was visible during the entire scanning session and provided a minimal depth cue in otherwise complete darkness. Three red point lights (targets) were interleaved in each row of blue point lights. Green point lights (fixation points) were placed centrally between rows, and were visible only one at a time. The foam board was situated on the subject's chest, such that its edge was near the chin. Foam padding was inserted in the head coil to minimize head movement and to tilt the head so that subjects could view the display directly without a mirror. The direct-view setup allows realistic depth perception under natural viewing conditions. The scanner room was completely darkened during the experiment. Each subject participated in four 512-s scans. During the first 512-s scan, subjects fixated the most distant fixation point while responding to targets with their right index finger. Starting from the first row near the chin, red-light targets (each lasting 500 ms) randomly appeared at three horizontal positions (left, middle or right) for 4 s and moved on to the second row for 4 s (Fig. 1). Subjects were instructed to attend to the depth where targets appeared and tap their index finger for each target detected. The locations of targets wrapped around in depth (phase-encoded; from near to far) every 32 s. The second 512-s scan was the same as the first except that the targets appeared from far to near every 32 s. The first and second scans were each repeated twice.

2.2.1. Implementation

Fig. 1 shows the schematic circuit diagram and spatial layout of the experimental setup. The circuits were designed in-house for this study. Programs written in ANSI C sent 8-bit binary codes to data pins (D0–D7) of a PC parallel port, which could turn on one of 256 lights at a time. The first paradigm required that both fixation points and targets be seen at the same time, which could be implemented by controlling the higher and lower data bits independently. The targets (red lights; r1–r24) were controlled by data pins D0–D4 using three '4-line to 16-line' decoders (74LS154 ICs; National Semiconductor, Santa Clara, CA), each of which decodes four-bit inputs and sends logic LOW to one of 16 mutually exclusive outputs. The fixation points (green lights; g1–g7) were controlled by data pins D5–D7 using another 74LS154 IC. In this experiment, the subject always fixated the most distant green light (g7), which was constantly visible during the scan. The configuration of multiple fixation
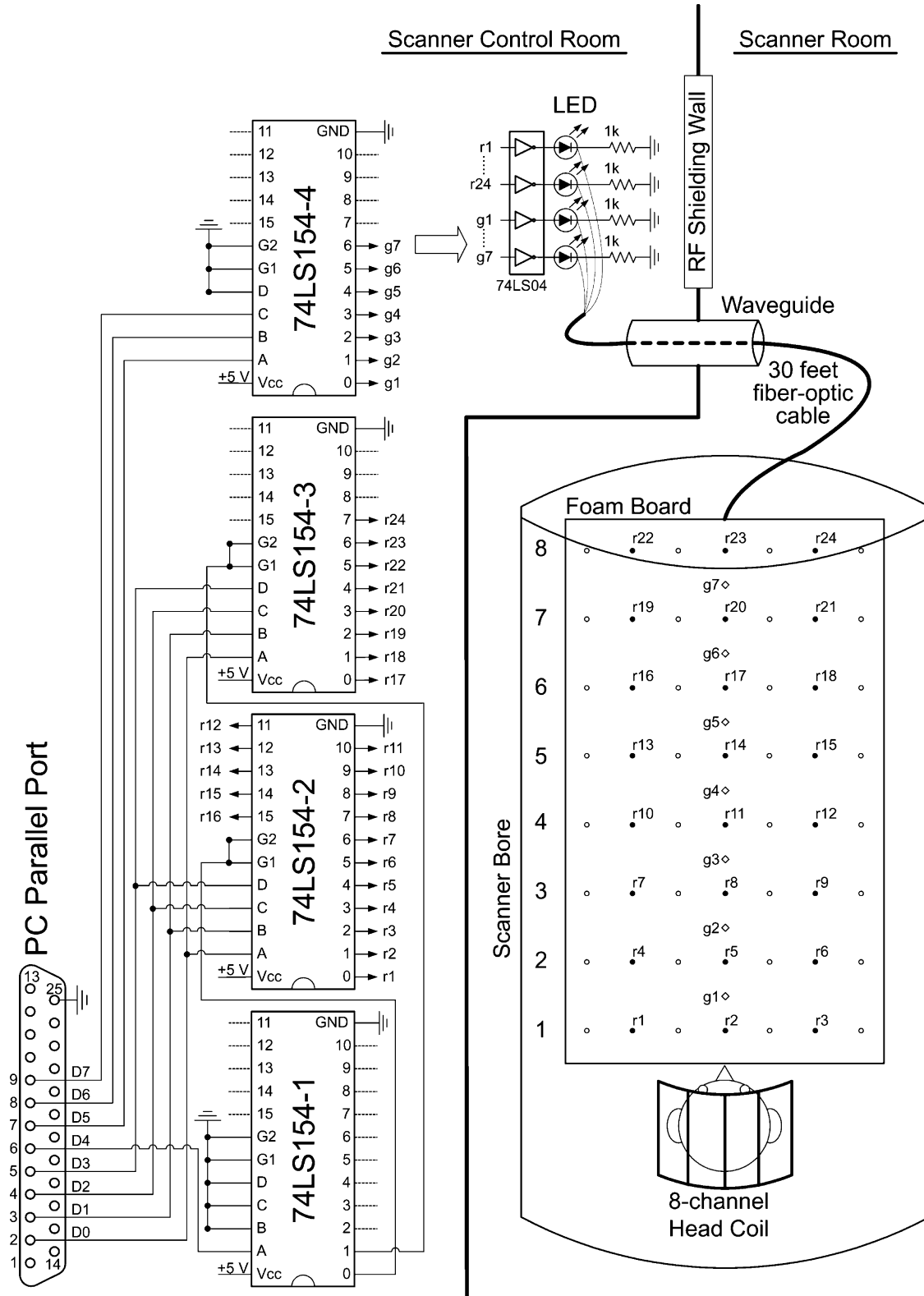
Fig. 1. Schematic diagrams of (left) decoding circuits and (right) experimental setup inside the scanner for Experiment I. Components were not drawn to scale. g#: number of green lights; r#: number of red lights; dashed lines on the ICs: unused pins; (on the foam board) open circles: blue lights; solid circles: red lights; open diamond: green lights.

points at different depth was used for another study reported elsewhere (Huang and Sereno, 2006). The outputs (r1–r24, g1–g7) of decoder ICs were inverted using hex inverting gates (74LS04 IC). A 30-ft, 64-strand fiber-optic cable (Part No. LG64-25; Fiber Optic Products, Inc., Clearlake Oaks, CA) was used to relay LED lights to the other end of the cable. Each strand of the cable is a 0.25 mm plastic optical fiber (POF) made from Polymethyl Methacrylate (PMMA) polymer. Although plastic optical fibers have higher transmission loss than glass fibers, they are low-cost, easy to implement, and suitable for short distance applications. One foot of the cable coating was peeled off to allow integration of individual fibers with LEDs. Homemade plastic connectors were used to align LEDs with one end of the optical fibers. Out of 64 fibers, 31 were used for targets and fixation points; 32 were used for the background light array and were constantly illuminated by a single blue LED (circuit not shown in Fig. 1); and the last strand was not used. The fiber-optic cable entered the scanner room via a waveguide on the RF shielding wall and reached the foam board inside the scanner bore. The coating of the last three feet of the cable was peeled off so that each strand of optical fiber could be freely connected to a pinhole on the foam board. Fig. 2 demonstrates a perspective view of the fiber-optic display in a dark room, in which only point lights were visible.
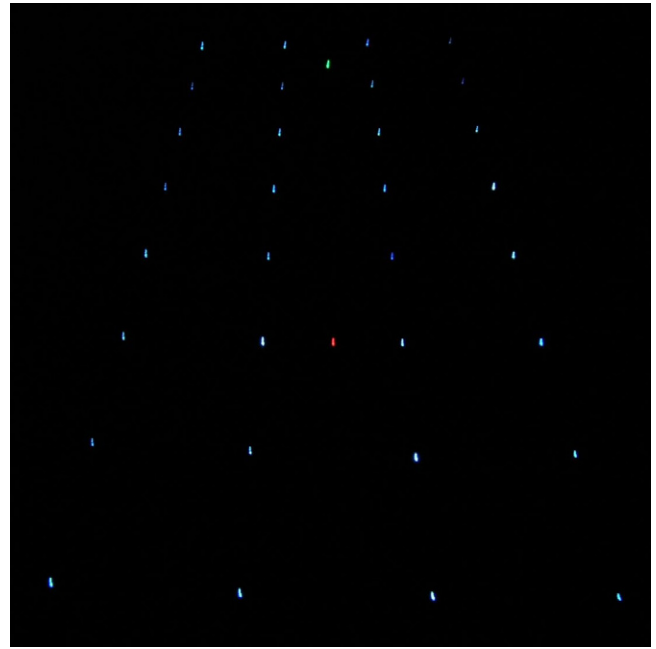

Fig. 2. A snapshot of the fiber-optic display in Experiment I (the photo was taken outside of the scanner room). A fixation point (green) and a point-light target (red) are visible in the middle of the display. (For interpretation of the references to color in this figure legend, the reader is referred to the web version of the article.)

2.3. Experiment II—delayed saccade task

Recent fMRI studies using the delayed saccade task have revealed topographic maps in human posterior parietal cortex (Sereno et al., 2001; Schluppeck et al., 2005). In these experiments, subjects viewed stimuli on a back-projection screen (or LCD) through an angled mirror. Here, a similar experimental paradigm was carried out using a fiber-optic based apparatus, where point-light stimuli were presented immediately adjacent

to the subject's face. Each subject participated in four 512-s functional scans. Each 512-s scan consisted of eight cycles of 64-s periods, each of which contained twelve 5.33-s trials. The stimuli included a central fixation point (red point light) and 12 peripheral targets (green point lights) evenly spaced in the visual field (Fig. 3a). A peripheral target (green point light) appeared between 1 and 1.5 s after the trial onset (Fig. 3b), and the subject
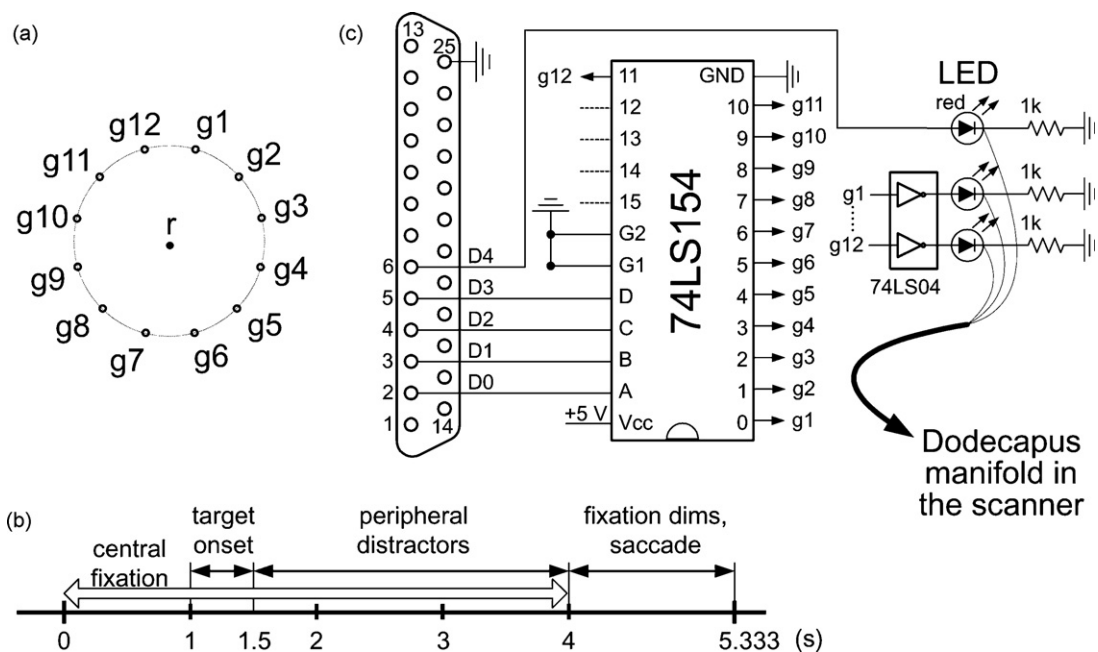

Fig. 3. Schematic illustrations of Experiment II. (a) Target locations, (b) timing of the delayed saccade task, and (c) circuit diagram.
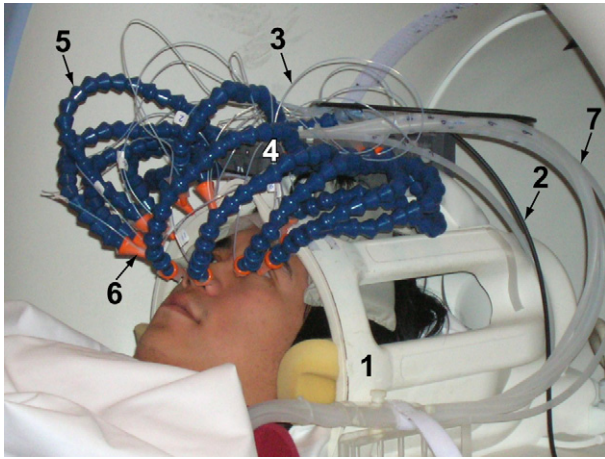
Fig. 4. Photograph of apparatus setup for Experiment II. (1) Head coil, (2) fiber-optic cable, (3) single-strand optical fiber enclosed in a thin plastic tube, (4) Dodecapus manifold, (5) flexible legs, (6) air-puff nozzles (tips), and (7) air tubes.

was required to remember the location of the target. During the delay period (between 1.5 and 4 s), distractors (green lights, each lasting 10 ms) randomly flashed at the 12 target locations. The subject fixated the red point light at the center for the first four seconds of the trial, and the red fixation was dimmed between 4 and 5.33 s of the trial. At the onset of fixation dimming and off-set of distractors, the subject made a saccade from the fixation point to the remembered target location in the periphery, and then made a saccade back to the central fixation and waited for the next target. In a 64-s cycle, the target appeared successively (phase-encoded) at 12 locations in a counterclockwise (CCW) or clockwise (CW) direction (Fig. 3a).

2.3.1. Implementation

The circuit diagram for experiment II (Fig. 3c) was a simplified version of experiment I. The targets (green lights; g1–g12) were controlled by data pins D0–D3 using one 74LS154 IC, whose outputs were inverted using two 74LS04 ICs. The fixation point (red light) was controlled directly by data pin D4. The 30-ft fiber-optic cable used for experiment II contained 32 strands of 0.5 mm plastic optical fibers (Part No. LG32-5; Fiber Optic Products, Inc., Clearlake Oaks, CA). Thirteen out of the 32 fibers were used for 12 targets and the fixation point. The fiber-optic cable entered the scanner room through a waveguide and reached a supporting structure, the Dodecapus manifold (Figs. 3c and 4). The manifold was originally designed to deliver air puffs to the face and lips in somatosensory experiments (see details in Huang and Sereno, 2007). Each flexible 'leg' of the manifold was made of segments of plastic modular hose (LOC-LINE; Lockwood Products, Inc., Lake Oswego, OR). The flexible leg could be readily used in the manner of a gooseneck lamp when a light source (e.g. LED or fiber-optic point light) is attached to its tip (a 1/16 in. round nozzle). Here, we simply attached the end point of a single-strand optical fiber to the tip of each leg (Fig. 4). Alternatively, optical fibers could also pass through the conduit inside the leg. The last two feet of cable coating were peeled off, and each segment of bare optical fiber was enclosed

in a thin plastic tube (∼1 mm) for protection. All 12 fibers carrying green lights (targets) were attached to 12 legs according to the spatial layout of Fig. 3a. A 'thirteenth' leg was added to support the central fixation point (red lights). The dimming of the fixation point was simulated by blinking the LED with a ∼0.025% duty cycle (5-μs ON vs. 20-ms OFF). A 5-inch plastic disc with labels of target locations (Fig. 3a) was used to assist the adjustment of legs during experimental setup. The tips of the legs (point lights) were about 5 cm from the eyes, resulting in a large visual angle near $100°$ ($\pm 50°$).

2.4. Data acquisition and analysis

fMRI experiments were conducted according to protocols approved by the Human Research Protections Program of the University of California, San Diego. All subjects had normal or corrected-to-normal vision. Each fMRI session consisted of four functional scans and one structural scan. Echo-planar images (EPI) were collected during 512-s functional scans (GE 3T short bore scanner, 8-channel head coil, single shot EPI, FOV = 20 cm, 3.125 mm × 3.125 mm in-plane, 4 mm thick slices, 256 images per slice, 31 axial slices, 64 × 64 matrix, flip angle = 90°, TE = 30 ms, TR = 2000 ms). Structural images (FSPGR, FOV = 25.6 cm, 1 mm × 1 mm in-plane, 1.3 mm thick slices, 106 axial slices, 256 × 256 matrix) were collected at the same plane as the functional scans. Functional scans were motion-corrected using AFNI 3dvol-reg (http://afni.nimh.nih.gov/afni). Data were analyzed using Fourier methods and significant activations were rendered on inflated or flattened cortical surfaces (Sereno et al., 1995, 2001). FreeSurfer (http://surfer.nmr.mgh.harvard.edu/download.html) was used to reconstruct the cortical surface for each subject from a pair of structural scans (FSPGR, 1 mm × 1 mm × 1 mm) acquired in a separate session. Fourier transform was performed for the time series at each voxel after removing the linear trend. An F-statistic was estimated by comparing the power at the stimulus frequency (8 or 16 cycles per scan) to the power of the noise (other frequencies) and converted to a p-value (uncorrected) by considering the degrees of freedom of signal and noise. The phase of periodic signal at the stimulus frequency was displayed using a continuous color scale (red → blue → green). The saturation of the colors was modulated by the p-value (after passing it through a sigmoid), as illustrated in the color bar insets in the figures, effectively thresholding the data.

3. Results

Here, we demonstrate the feasibility of fiber-optic stimulus presentation with results from one representative subject for each experiment. Fig. 5 shows results of Subject 1 in Experiment I. Significant periodic activities ($p < 0.01$, uncorrected) at the stimulus frequency (16 cycles/scan) and their phases were rendered on a flattened cortical surface of the right hemisphere. A cut was made at the fundus of calcarine sulcus, approximately dividing the upper (V1+) and lower fields (V1−) of the primary visual cortex. The borders of visual areas V1, V2, V3, V3A, VP, and V4v were defined by retinotopic mapping paradigms (Sereno et
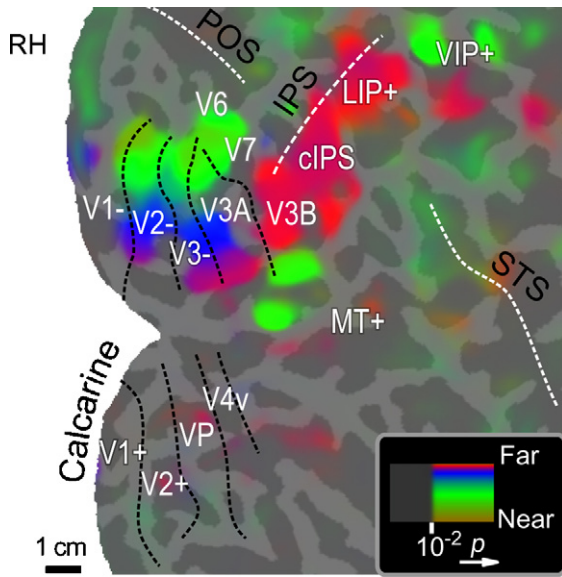
Fig. 5. Results of Experiment I (subject 1). POS: parieto-occipital sulcus. IPS: intraparietal sulcus; STS: superior temporal sulcus; cIPS: caudal IPS; LIP+: lateral IPS; VIP+: ventral IPS; white dashed lines: fundus of major sulcus; black dashed lines: borders between visual areas. The 'plus' signs of LIP+, VIP+, and MT+ indicate multiple subdivisions, while the 'plus' signs of V1+ and V2+ indicate upper visual field.
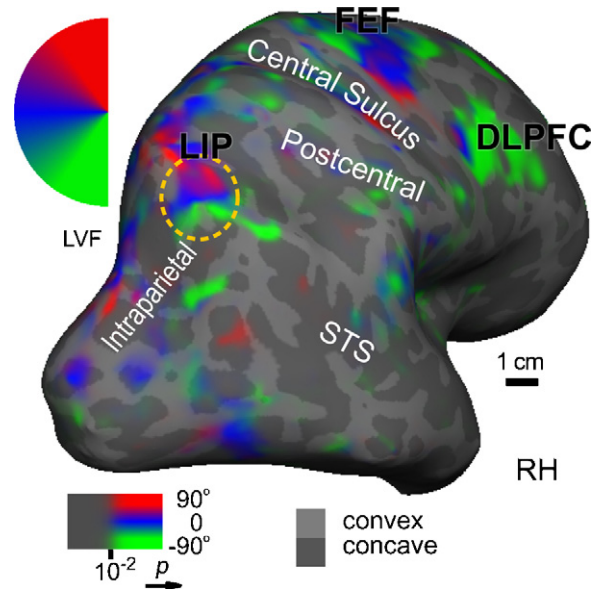

Fig. 6. Results of Experiment II (subject 2). The color-wheel indicates the polar angle representation of the left visual field (LVF). (For interpretation of the references to color in this figure legend, the reader is referred to the web version of the article.)

al., 1995; Pitzalis et al., 2006) in a separate functional session from the same subject. In Experiment I, the subject fixated the most distant green point light, and attended to targets appearing progressively at different depths in the center of the lower visual field. The distal targets (far) are expected to activate cortical representation of parafoveal eccentricity, while the proximal targets (near) are expected to activate peripheral eccentricity. The resulting topographic maps in Fig. 5 are consistent with retinotopic locations of the targets. The early visual areas (V1, V2, V3 and V3A) showed activities in areas near the vertical meridian representation (V1/V2 and V3/V3A borders) of the lower visual field. The activation in area V1 was confined to a thin strip at the V1/V2 border, which could be explained by the tiny visual angle of the targets (point lights) and the small size of receptive fields in V1. There was almost no periodic activation in areas of the upper field representation (V1+, V2+ and VP). The topographic representation of depth (far to near; color-coded as red → blue → green) was consistent with the gradient direction of eccentricity (parafoveal to peripheral) in early visual areas. Additional non-topographical activations (either near or far representations) were found beyond early visual areas (Fig. 5), including two areas between V3B and MT+, and a few areas lateral to the intraparietal sulcus (IPS). These areas were not activated using back-projection approaches as in our previous retinotopic experiments. Some of these areas may correspond to areas activated using stereopsis and stimuli with surface orientation in other studies (Shikata et al., 2001; Tsao et al., 2003). The labels of these additional areas are tentative and their functions and precise locations will be reported and discussed elsewhere.

Fig. 6 shows results (subject 2) from Experiment II. Significant periodic activities ($p < 0.01$, uncorrected) at the stimulus frequency (8 cycles/scan) and their phases were rendered on

an inflated cortical surface (posterior-lateral view) of the right hemisphere. The delayed saccade paradigm revealed topographic maps of polar angle of contralateral (left) hemifield in lateral intraparietal sulcus (LIP), frontal eye fields (FEF), and dorsal lateral prefrontal cortex (DLPFC). The location and topographic map of area LIP (as indicated by a dashed circle in Fig. 5) was consistent with the result in Sereno et al. (2001). Additional activation was found anterior and medial to area LIP, which was consistent with recent evidence of multiple topographic maps along the intraparietal sulcus (Schluppeck et al., 2005; Swisher et al., 2007). Although point-light targets were presented near the face, weak activation was found in area VIP+, which responds to near-face multisensory stimuli (Sereno and Huang, 2006).

4. Discussion

fMRI is a noninvasive technique useful for mapping human brain function. However, limited space and strong magnetic fields impose constraints on experiments that could be conducted inside an MRI scanner. The safety of human subjects is always the top priority when one designs experiments and implements devices for the MRI environment. From a preventive perspective, metallic objects (both ferromagnetic and non-ferromagnetic), electronic and mechanical components, and conductive wires must be avoided whenever possible. In addition to safety issues, all stimulus presentation and response monitoring devices must be compatible with MRI and should not result in imaging artifacts. Furthermore, the stimulus or response signals traveling through conductive wires could be disrupted by fast varying gradient fields and RF pulses.

In this study, we explored the feasibility of visual stimulus presentation using fiber optics in the MRI scanner. The fiber-optic display does not contain conductive wires or ferromagnetic

materials and can be readily installed in the MRI scanner without additional precautions. The design and construction of a fiber-optic stimulus presentation apparatus consist of three elements, including software programs for controlling the timing and sequence of stimuli, digital circuits for decoding signals from the parallel port, and structures for supporting individual or arrays of fiber-optic lights. These elements need to be modified according to the specification of each experimental paradigm, which could be a potential disadvantage compared with the conventional visual stimulus presentation using back-projection approaches. The digital circuits for decoding binary signals can be reused for different experiments without modification. Any software (e.g. C, Matlab®, or Presentation®) with functions controlling PC parallel ports can be used to command the digital circuit. The programming effort would be less or comparable to programming visual stimuli on conventional displays. The supporting structures, however, need to be redesigned and constructed for different experiments.

The existing back-projection approach widely used by the fMRI community, on the contrary, only requires programming for visual stimuli and it is easy to setup the video projector, screens, and mirrors during experiments. Therefore, we consider the fiber-optic approach only a complement and optimal for experiments that are difficult or impossible to setup using the back-projection approach. The apparatus in Experiment I presented point-light targets along a slanted surface extending a few feet from the subject's chin to the knees. This spatial arrangement could not be implemented using the back-projection approach. Results in Experiment I showed that a few new areas lateral to the intraparietal sulcus were activated by realistic 3-D targets at different depths. Results in Experiment II suggested that phase-encoded topographic mapping paradigms could be implemented using fiber-optic based displays with a small number (13) of fiber-optic point lights. We showed that the results were consistent with experiments using the back-projection approach (Sereno et al., 2001).

Because of limited space for the supporting structure inside the scanner bore and the size of the data port (8-bit) of a PC parallel port, the number of individual fiber-optic lights that could be presented is on the order of one hundred, which is considerably fewer than LCD projectors and fiberscopes (on the order of one million pixels). However, our fiber-optic approach allows targets to be flexibly presented at any 3-D location inside the scanner bore, providing realistic depth perception under natural viewing conditions. Subjects could view the stimuli directly without a mirror, and perform goal-directed visuomotor tasks in their peripersonal space (Chapman et al., 2007; Filimon et al., 2007; Quinlan and Culham, 2007; Culham et al., 2008). The direct-view solution is also related to another limitation on visual stimulus presentation near a head coil. The field of view is restricted (10°–20°) when the subject views visual stimuli on a back-projection screen through an angled mirror. The dimension of the screen and the mirror is confined to the available space around the head coil. In this study, the integration of the Dodecapus manifold and optical fibers (Fig. 4) makes it possible to present point-light targets near the face inside or near the head coil, which could be useful for studying cortical represen-

tation of peripheral space (Scott et al., 2003; Pitzalis et al., 2006; Sereno and Huang, 2006).

Finally, we will discuss other potential designs and applications for fiber-optic based displays in an MRI environment. First, apparent motion or optic flow patterns could be simulated by rapid serial presentation of adjacent point lights in a row or an array. In a pilot study, we have simulated a point light moving toward or away from the subject on the light array. Second, the fiber-optic light array could be distributed on any two- or three-dimensional supporting surface to simulate surface orientation and texture gradient (Shikata et al., 2001). Third, the color of each LED was fixed in this study. In further studies, dual- or tri-color LEDs may be used to increase stimulus complexity or used for fMRI research on color perception. Fourth, the fiber-optic approach allows visuomotor activities in complete darkness following the brief presentation of point-light targets. For instance, the subject can reach to a cued location in 3-D space with or without the sight of his or her own hand, thereby resolving the confounds introduced by background illumination of an LCD projector (Filimon and Sereno et al., in preparation). Fifth, the apparatus for Experiment II can readily be used for multisensory experiments, where tactile (air puffs) and visual (point lights) stimuli are delivered simultaneously at the tips of the Dodecapus legs. Originally, our multisensory stimuli were generated by aligning a back-projection screen with the air-puff nozzles in front of the subject's face (Sereno and Huang, 2006). Similar setup of bimodal stimuli (air puffs plus lights) has been demonstrated in eyeblink conditioning (EBC) paradigms in animal fMRI experiments (Li et al., 2003; Miller et al., 2005). Furthermore, the Dodecapus manifold may be integrated with another fiber-optic system for tracking eye movements (Kimmig et al., 1999; Kanowski et al., 2007) or monitoring motor responses (Meinhardt and Müller, 2001).

Acknowledgements

References

Armenean C, Perrin E, Armenean M, Beuf O, Pilleul F, Saint-Jalmes H. RF-induced temperature elevation along metallic wires in clinical magnetic resonance imaging: influence of diameter and length. Magn Reson Med 2004;52:1200–6.

Brau AC, Wheeler CT, Hedlund LW, Johnson GA. Fiber-optic stethoscope: a cardiac monitoring and gating system for magnetic resonance microscopy. Magn Reson Med 2002;47:314–21.

Burdet E, Gassert R, Gowrishankar G, Chapuis D, Bleuler H. fMRI compatible haptic interfaces to investigate human motor control. In: Proc. 9th international symposium on experimental robotics (ISER); 2004.

Chapman H, Pierno AC, Cunnington R, Gavrilescu M, Egan G, Castiello U. The neural basis of selection-for-action. Neurosci Lett 2007;417:171–5.

Cornelissen FW, Pelli DG, Farell B, Huckins SC, Szeverenyi NM. A binocular fiberscope for presenting visual stimuli during fMRI. Spat Vis 1997;11:75–81.

Crisp J. Introduction to fiber optics. 2nd ed. Oxford: Newnes Press; 2001.

Culham JC, Valyear KF. Human parietal cortex in action. Curr Opin Neurobiol 2006;16:205–12.

Culham JC, Cavina-Pratesi C, Singhal A. The role of parietal cortex in visuomotor control: what have we learned from neuroimaging? Neuropsychologia 2006;44:2668–84.

Culham, JC, Gallivan, J, Cavina-Pratesi, C, Quinlan, DJ. fMRI investigations of reaching and ego space in human superior parieto-occipital cortex. In: Klatzky RL, Behrmann M, MacWhinney B, editors, Embodiment, ego-space and action. Madwah, NJ: Erlbaum, 2008.

DeCusatis CM, DeCusatis CJS. Fiber optic essentials. Amsterdam: Elsevier/Academic Press; 2006.

Dempsey MF, Condon B. Thermal injuries associated with MRI. Clin Radiol 2001;56:457–65.

Dempsey MF, Condon B, Hadley DM. Investigation of the factors responsible for burns during MRI. J Magn Reson Imaging 2001;13:627–31.

Engel SA, Rumelhart DE, Wandell BA, Lee AT, Glover GH, Chichilniski EJ, Shadlen MN. FMRI of human visual cortex. Nature 1994;369:525.

Filimon F, Nelson JD, Hagler Jr DJ, Sereno MI. Human cortical representations for reaching: mirror neurons for execution, observation, and imagery. NeuroImage 2007;37:1315–28.

Goff DR. Fiber optic reference guide: a practical guide to communications technology. 3rd ed. Amsterdam: Elsevier/Focal Press; 2002.

Greatbatch W, Miller V, Shellock FG. Magnetic resonance safety testing of a newly-developed fiber-optic cardiac pacing lead. J Magn Reson Imaging 2002;16:97–103.

Hoffman HG, Richards TL, Magula J, Seibel EJ, Hayes C, Mathis M, Sharar SR, Maravilla K. A magnet-friendly virtual reality fiberoptic image delivery system. Cyberpsychol Behav 2003;6:645–8.

Huang RS, Sereno MI. Dodecapus: an MR-compatible system for somatosensory stimulation. NeuroImage 2007;34:1060–73.

Huang RS, Sereno MI. Mapping cortical representations of body-centered distance using MR-compatible fiber optics. 36th annual meeting of the society for neuroscience, Atlanta, Georgia; 2006.

Kanowski M, Rieger JW, Noesselt T, Tempelmann C, Hinrichs H. Endoscopic eye tracking system for fMRI. J Neurosci Methods 2007;160:10–5.

Kimmig H, Greenlee MW, Huethe F, Mergner T. MR-eyetracker: a new method for eye movement recording in functional magnetic resonance imaging. Exp Brain Res 1999;126:443–9.

Lagopoulos J, Malhi GS, Shnier RC. A fiber-optic system for recording skin conductance in the MRI scanner. Behav Res Methods 2005;37:657–64.

Li L, Weiss C, Disterhoft JF, Wyrwicz AM. Functional magnetic resonance imaging in the awake rabbit: a system for stimulus presentation and response detection during eyeblink conditioning. J Neurosci Methods 2003;130:45–52.

Lindberg LG, Ugnell H, Oberg PA. Monitoring of respiratory and heart rates using a fibre-optic sensor. Med Biol Eng Comput 1992;30:533–7.

Meinhardt J, Müller J. Motor response detection using fiber optics during functional magnetic resonance imaging. Behav Res Methods Instrum Comput 2001;33:556–8.

Miller MJ, Li L, Weiss C, Disterhoft JF, Wyrwicz AM. A fiber optic-based system for behavioral eyeblink measurement in a MRI environment. J Neurosci Methods 2005;141:83–7.

Pitzalis S, Galletti C, Huang RS, Patria F, Committeri G, Galati G, Fattori P, Sereno MI. Wide-field retinotopy defines human cortical visual area V6. J Neurosci 2006;26:7962–73.

Quinlan DJ, Culham JC. fMRI reveals a preference for near viewing in the human parieto-occipital cortex. Neuroimage 2007;36:167–87.

Sade S, Katzir A. Fiberoptic infrared radiometer for real time in situ thermometry inside an MRI system. Magn Reson Imaging 2001;19:287–90.

Savoy RL, Ravicz ME, Gollub R. The psychophysiological laboratory in the magnet: stimulus delivery, response recording, and safety. In: Moonen CTW, Bandettini PA, editors. Functional MRI. Berlin: Springer-Verlag; 1999. p. 347–65.

Schluppeck D, Glimcher P, Heeger DJ. Topographic organization for delayed saccades in human posterior parietal cortex. J Neurophysiol 2005;94:1372–84.

Scott GD, Dow MW, Neville HJ. Human retinotopic mapping of the far periphery. 33th annual meeting of the society for neuroscience, New Orleans, Louisiana; 2003.

Sereno MI, Huang RS. A human parietal face area contains aligned head-centered visual and tactile maps. Nat Neurosci 2006;9:1337–43.

Sereno MI, Dale AM, Reppas JB, Kwong KK, Belliveau JW, Brady TJ, Rosen BR, Tootell RB. Borders of multiple visual areas in humans revealed by functional magnetic resonance imaging. Science 1995;268:889–93.

Sereno MI, Pitzalis S, Martinez A. Mapping of contralateral space in retinotopic coordinates by a parietal cortical area in humans. Science 2001;294:1350–4.

Shellock FG. Magnetic resonance safety update 2002: implants and devices. J Magn Reson Imaging 2002;16:485–96.

Shikata E, Hamzei F, Glauche V, Knab R, Dettmers C, Weiller C, Buchel C. Surface orientation discrimination activates caudal and anterior intraparietal sulcus in humans: an event-related fMRI study. J Neurophysiol 2001;85:1309–14.

Strasburger H, Wüstenberg T, Jäncke L. Calibrated LCD/TFT stimulus presentation for visual psychophysics in fMRI. J Neurosci Methods 2002;121:103–10.

Swisher JD, Halko MA, Merabet LB, McMains SA, Somers DC. Visual topography of human intraparietal sulcus. J Neurosci 2007;27:5326–37.

Tsao DY, Vanduffel W, Sasaki Y, Fize D, Knutsen TA, Mandeville JB, Wald LL, Dale AM, Rosen BR, Van Essen DC, Livingstone MS, Orban GA, Tootell RB. Stereopsis activates V3A and caudal intraparietal areas in macaques and humans. Neuron 2003;39:555–68.

Zakzanis KK, Mraz R, Graham SJ. An fMRI study of the trail making test. Neuropsychologia 2005;43:1878–86.